Cellularized Collagen-Membrane Lung Assist Devices for Efficient Gas Transfer

Abstract

Chronic lower respiratory disease afflicts over 5% of the United States population, leading to over 145,000 deaths annually. There remains a need for safer and more durable alternatives to lung transplant for patients who progress to end-stage lung disease. Portable or implantable gas oxygenators based on microfluidic technologies can address this need, though harnessing their potential depends on efficient and biocompatible design. Incorporating biomimetic materials into such devices can help replicate efficient native gas exchange function and additionally support cellular components. In this work, we developed microfluidic devices that enable blood gas exchange across ultra-thin collagen membranes (as thin as 2 μm). Endothelial, stromal, and parenchymal cells readily adhere to these membranes, and long-term culture with cellular components results in membrane remodeling, reflected by reductions in membrane thickness. Functionally, these collagen-membrane lung devices in the acellular configuration mediated effective gas exchange up to rates of ~288 mL/min/m^2 O_2 transfer and ~685 mL/min/m^2 CO_2 transfer, approaching the gas exchange efficiency measured in the native lung. After testing several configurations of lung devices to explore various physical parameters of the device design, we concluded that thinner membranes and longer gas exchange distances result in improved hemoglobin saturation and increases in pO_2. However, in the design space tested, these effects were relatively small compared to the improvement in overall oxygen and carbon dioxide transfer by increasing the blood flow rate – limited primarily by shear forces experienced by blood components. Finally, collagen-membrane devices cultured with endothelial and parenchymal cells achieved similar gas exchange rates compared with acellular devices. Biomimetic blood oxygenator design opens the possibility of creating portable or implantable microfluidic devices that achieve efficient gas transfer while also maintaining physiologic conditions.

Table of Contents

List of Figures and Tables

1 Background

1.1 Burden of chronic lung disease

Chronic lower respiratory diseases such as chronic obstructive pulmonary disease (COPD) affect over 5% of the U.S. population, causing 145,000 deaths annually and comprising the third leading cause of death.[1] For patients who progress to end-stage lung disease, lung transplantation remains the best treatment option for eligible candidates. While the number of lung transplants performed annually has continued to increase year after year, 11% of patients who enter the U.S. lung transplant list die before transplantation, reflecting the ongoing shortage of organs.[2] Based on the latest available figures for patients listed in 2015, the median wait time has decreased to 3.4 months overall,[3] but this continues to exceed the short-term scope of most technologies available to support patients with respiratory failure, as discussed in Section 1.2. Furthermore, the waitlist mortality rate was 16.5 deaths per 100 waitlist years in 2015, nearly double the mortality rate in 2004-2005.[3] Thus, there is an ongoing need for portable or implantable devices that assist with gas exchange in patients who are awaiting transplant, whose transplants are failing, or for whom transplant is contraindicated.

1.2 Current management of respiratory failure

Chronic lower respiratory disease is currently typically managed with conservative measures appropriate for the etiology, *e.g.* corticosteroids and supplemental oxygen for COPD and supplemental oxygen for interstitial pulmonary fibrosis (IPF). However, exacerbations or gradual worsening of chronic lung disease in the setting of limited respiratory reserve, as well as acute respiratory decompensation in conditions such as acute respiratory distress syndrome (ARDS) or severe pneumonia, necessitate hospitalization and sometimes ICU admission. There is often interplay between these different causes of respiratory decompensation, as chronic disease can predispose a patient to the latter acute events. Regardless, with irreversible decline

in lung function, the long-term goal eventually becomes bridging the patient to a first or repeat lung transplant.

In patients with potentially reversible respiratory failure for whom conservative measures have failed, technologies for supporting gas exchange function are available, though they are essentially restricted to short-term use. Patients may be ventilated through non-invasive (*e.g. via* face-mask) or invasive mechanical ventilation (*e.g. via* endotracheal intubation). In patients whose conditions are refractory to mechanical ventilation, extracorporeal membrane oxygenation (ECMO) may be employed such that blood is removed from the body and directly oxygenated across artificial membranes, replacing native lung function.[4] Specific configurations are selected based on the scenario, with veno-venous (VV) ECMO being appropriate for isolated compromise of lung function (*e.g.* ARDS or failed lung transplantation) and veno-arterial (VA) ECMO being appropriate for patients who additionally have compromised cardiac function requiring bypass. However, there are significant complications from ECMO, largely because the device subjects blood to contact with bare membranes at unphysiologically high shear stresses. The elevated risk of thrombotic events necessitates anticoagulation with heparin or newer agents that leads to bleeding complications in a substantial proportion (8-56% depending on aPTT target) of patients undergoing the procedure, as well as a risk of developing heparin-induced thrombocytopenia if heparin is used.[5, 6] Even with anticoagulation, thrombotic events are estimated to still occur in up to 53% of cases, in a trade-off with bleeding risk, as studied in a systematic review of VV-ECMO.[5] As such, ECMO carries a high mortality risk and is rarely used for greater than several weeks consecutively, making it unviable for long-term or outpatient settings.[7] Indeed, while ECMO has seen success and widespread use in treatment of neonatal respiratory distress, where survival rates are around 74% as reported by the Extracorporeal Life Support Organization, adult cases showed a lower 58% rate of survival to discharge with an average treatment duration of ~12 days.[8]

Newer devices, such as the Hemolung and Novalung approved for use in international settings, utilize alternate architectures and have successfully bridged patients to transplant.[9, 10] The Hemolung, first used in the United States in 2015, utilizes a cartridge in which blood is propelled by a rotating impeller in the plane normal to a bundle of hollow gas-flow fibers coated with heparin on the blood-facing surface.[11] The Novalung Interventional Lung Assist (iLA), in contrast, is a pumpless device using a low-resistance membrane for gas exchange; there is a case report of its use over 140 consecutive days.[9] Marketed as low-flow rate extracorporeal carbon dioxide removal ($ECCO_2R$) systems, these aforementioned technologies are primarily useful in hypercapnic respiratory failure and are not equipped to manage hypoxemic conditions or those requiring full cardiopulmonary support.[4] They can reduce dependency on mechanical ventilation but frequently cannot replace mechanical ventilation altogether. Furthermore, these devices still require monitoring for thrombus formation, and no randomized controlled trials have yet demonstrated reductions in complications. Engineering lung assist devices with biomimetic materials, cellular components, and physiologic blood flow profiles as we propose in this work can promote self-maintenance while reducing the risk of coagulation, enabling the use of such devices in long-term outpatient therapy as well as efficient gas exchange that can relieve hypoxemia in addition to hypercarbia.

1.3.1 Fabrication approaches to creating lung assist devices

Broadly speaking, there are two approaches to creating next-generation lung assist devices and artificial lungs. The first strategy is to rationally design and fabricate microfluidic networks of vascular and respiratory channels (**Figure 1-1A**), typically using gas-permeable polymer materials such as polycarbonate (PC) or poly(dimethylsiloxane) (PDMS) to form a membrane between blood and air.[12-16] This strategy is the natural miniaturized extension of the engineering principles behind ECMO, Hemolung, and Novalung – and indeed more broadly the

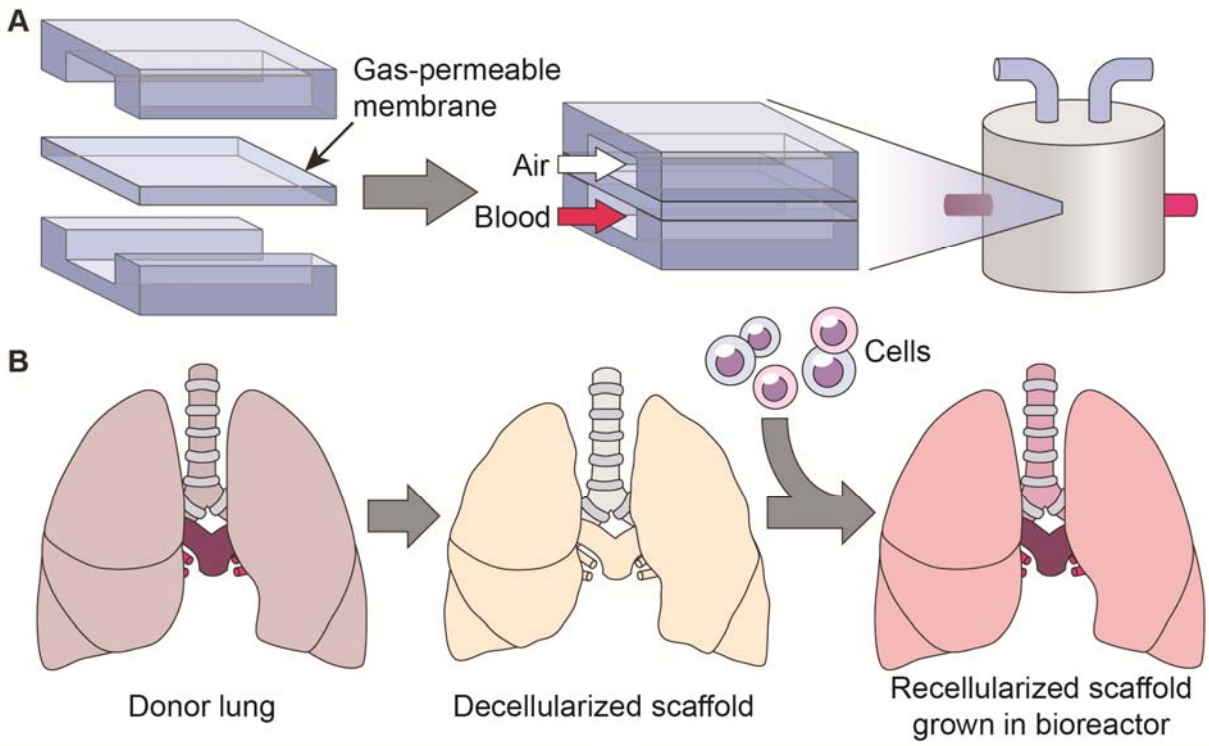

Figure 1-1. Experimental approaches to replacing lung function. (A) Generic depiction of microfluidic device wherein blood is oxygenated across an artificial respiratory membrane, connected to the host as an external device. **(B)** General strategy for generating tissue engineered lungs through use of a decellularized scaffold seeded by donor-derived cells towards transplant into the host.

concept behind the organ-replacing technologies in widespread clinical use, such as hemodialysis and cardiopulmonary bypass machines.

The Mockros group has employed photolithographic techniques to make microfluidic arrays of sub-millimeter (300 μm wide x 15 μm deep) blood channels separated from gas chambers by a 130 μm-thick polycarbonate layer, achieving an oxygen flux of 7-10x10^{-7} mol/(min-cm^2 membrane).[13] The Ingber group has developed “lung-on-a-chip” technology, recapitulating both small airways[17] and the alveolar-capillary interface[15] through tissue culture on thin PDMS membranes rigged to stretch and contract analogously to lung inflation *in vivo*. The intended applications have been in modeling lung pathophysiology (*e.g.* COPD exacerbation) and drug response/toxicity rather than serving as lung assist devices. Finally, the Borenstein group has designed multi-layer microfluidic devices that incorporate sophisticated

channel branching architectures so as to replicate natural vasculature patterns; gas exchange was mediated across relatively thin (down to 11 μm) PDMS membranes.[18]

These approaches have the advantage of enabling consistent high-efficiency gas exchange by affording control of physical parameters such as membrane durability and gas/liquid flow rates, and they do not necessarily require any living components to operate. However, introduction of extensive foreign material or operation under unsuitable hemodynamic flows and vessel geometries will still sacrifice biocompatibility and promote life-threatening thrombosis. Furthermore, as with any artificial device, long-term maintenance presents a challenge, particularly if the device is to be implanted internally.

1.3.2 Native scaffold approaches for lung tissue engineering

The second general strategy is to establish or isolate ECM-based environments and seed these scaffolds with cells which self-pattern and differentiate into mature lung structures in a bioreactor prior to transplantation (**Figure 1-1B**).[19-22] This approach makes use of the native architecture to better replicate physical conditions that blood components will tolerate, as well as provide a substrate that could potentially be maintained and repaired indefinitely by the appropriate cell populations. Practical challenges include (1) avoiding/repairing defects in the re-created vasculature and parenchyma that could lead to serious leaks, (2) ensuring the quality of decellularization to avoid immune reactions, (3) minimizing the risk of infection from pathogens potentially introduced during the processing and incubation of the re-cellularized scaffold, and (4) generating patient-derived cell populations capable of re-seeding the scaffold.

Seeding of artificial ECM-inspired scaffolds has yielded epithelial and Type II pneumocyte-like cells in alveolus-like configurations; however, these efforts have not to date been tested for gas exchange function.[21] Decellularized rat lungs have been used as natural ECM scaffolds, and when repopulated with proof-of-concept epithelial (neonatal rat lung epithelial cells) and lung endothelial cells, can be transplanted orthotopically and maintain

function for several hours.[19, 20] The decellularized lung scaffold approach, more recently demonstrated in nonhuman primates to promote reseeding by mesenchymal stem cells,[23] creates artificial lungs that are grossly and histologically lung-like.

Cell sourcing has emerged as a particularly daunting challenge. There are numerous distinct cell phenotypes in the mature lung (such as endothelial cells, smooth muscle cells, Type I and Type II pneumocytes, ciliated bronchial epithelium, mucus-secreting cells, alveolar macrophages, and chondrocytes), all of which have arguably indispensable functions. Thus, reconstitution of the appropriate cells requires both appropriate stem cell types and adequate regenerative/proliferative potential prior to or during the seeding and bioreactor phases. Advances in the derivation of key cell types via *in vitro* differentiation of induced pluripotent stem cells (iPSCs) or embryonic stem cells (ESCs) have enabled the creation of appropriate progenitors from easily-accessible patient-specific cells (skin, peripheral blood samples, or mesenchymal stem cells).[24] One intriguing variation of this approach has been to form embryonic-like organoids from human ESCs *in vitro* and allow them to develop and mature after engraftment in a living host. Such a procedure can regenerate histologically mature lung structures, but there are considerable logistical hurdles to making this a viable alternative to transplant.[25] Alternatively, cells may be derived from adult stem cells; the Ott group has recently used expanded human airway basal cells ($KRT5^{+}TP63^{+}$) in conjunction with primary human pulmonary endothelial cells to repopulate a decellularized rat lung (requiring on the order of 10^{8} cells; by comparison, the human lung probably contains on the order of 10^{11} cells).[26, 27] Such airway basal cells differentiate at minimum into Type I and II pneumocytes and bronchiolar secretory cells.[26]

Nevertheless, physical constraints inherent from the scaffold limit both modularity and the engineering tools available to ensure continuous function and maintenance. For instance, small defects in the scaffold (particularly in the gas exchange membrane), unmasked by decellularization or formed by incomplete recellularization or improper remodeling, would be

difficult to detect and repair. Additionally, while it is fairly straightforward to reconstitute monolayer alveolar capillaries and alveolar pneumocyte walls, the larger airways and vessels are considerably more complicated structures to properly recreate with a “hands-off” recellularization approach. Issues of defects and non-uniformity, as well as large-scale tissue- and organ-level organization, may benefit from the greater engineering control afforded by the use of some synthetic material and manufacturing techniques as introduced in section 1.3.1.

1.4 Approach in this work

Acknowledging the strengths of each approach presented above in sections 1.3.1 and 1.3.2, we decided to employ a hybrid construction in which a planned, fabricated network is composed of materials amenable to sustaining cellular components. Specifically, this thesis presents a prototypic biomimetic lung assist device based on gas exchange across an ultra-thin collagen membrane, with blood flowing in microfabricated vascular networks developed previously by our group.[28] We have tested such devices in acellular configurations as well as after population of the membrane with parenchymal and endothelial cells. Endothelial cells have been shown in the literature to reduce thrombogenicity of a synthetic gas exchange membrane,[29] and we believe that integrating these cells with a collagen membrane and parenchymal cells further enables plasticity and sustainability of the system. Since the collagen film functions analogously to the basement membrane between pneumocytes and endothelial cells in the physiologic setting, such a device has potential to facilitate efficient gas exchange while maintaining a biocompatible environment.

2 Materials and Methods

2.1 Overview of devices

Two types of microfluidic devices were designed and manufactured in this work: preliminary work used single-channel transwell devices (**Figure 2-1**), and subsequent iterations used multi-channel collagen-membrane gas exchange devices (all other figures). In both models, blood flowing in vascular channels was separated from an upper air chamber by a thin collagen membrane, but the techniques for manufacture and gas exchange testing differ.

2.2 Manufacture and gas exchange testing of single-channel transwell devices

A thin collagen membrane (45 μm thick) was created by air-drying a slurry of fibrillar bovine collagen. The collagen membrane was dehydrothermally crosslinked, then sterilized with ethylene oxide. To create the single-channel model, the collagen membrane was mounted in the place of the standard membrane in a 24-well plate transwell. Transwells with a polycarbonate membrane of 0.4 μm pore size and 10 μm thickness were used as controls.

Human umbilical vein endothelial cells (HUVECs) were seeded on the bottom of the collagen or polycarbonate membranes of the transwells and Human Type II pneumocytes (H441 cell line) were seeded on the top side (n=3 for both collagen and control membranes). In the controls, the bottom of the collagen membrane was seeded with HUVECs or fibroblasts (NIH-3T3 cell line) (n=3 for both cell types). Cells were cultured under standard conditions for two weeks.

Devices were assembled by affixing the transwell to the poly(dimethylsiloxane) (PDMS; Sylgard 184, Dow Corning) layers, with the membrane forming the top wall of the single 250 μm-deep vascular channel and air filling the transwell chamber above the membrane, as depicted in **Figure 2-1**. Computational fluid dynamics analysis was performed using COSMOSFloWorks™ (SolidWorks) to evaluate the device, estimating pressures on the order of

1 mmHg in the air chamber and 10 mmHg in the channel. The blood flow rate of 0.0625 mL/min was selected to correspond to 1 dyn/cm^2 shear stress based on this modeling.

Gas exchange testing of transwells was performed by pumping anticoagulated sheep blood (1% heparin, Lampire Biologics) with a syringe pump through the channel adjacent to the membrane of the transwell with oxygen flowing into and out of the top of the transwell (100 mL/min). Blood gas analysis was performed on the flowing blood before and after flowing past the transwell using a blood gas analyzer (Rapidlab 840, Chiron Diagnostics, Medfield, MA). n=3 per condition.

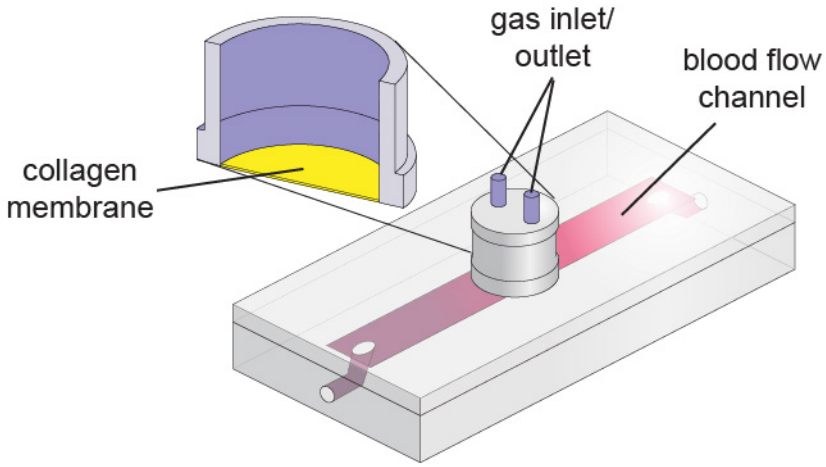

Figure 2-1. Schematic of single-channel transwell device with blown-up detail showing location of the collagen membrane. Parenchymal cells are seeded on the superior face of the membrane, while endothelial cells are seeded on the inferior face, in contact with the microfluidic channel.

2.3 Manufacture of multi-channel gas exchange devices

Multi-channel gas exchange devices consisted of three PDMS layers: a square-channel vascular layer, an air chamber layer, and a lid (**Fig. 2-2A**). The vascular and air chamber layers were designed in SolidWorks (SolidWorks, actual layout of 100-μm channel is displayed in **Fig. 2-2B**), and photolithography molds of these layers were produced on 10-cm silicon wafers (Stanford Microfluidics Foundry) and duplicated as polyurethane molds using Smooth-Cast 300 (Smooth-On). The vascular and air chamber layers were cast using standard soft lithography techniques. Air chamber layers were processed by using a scalpel to introduce

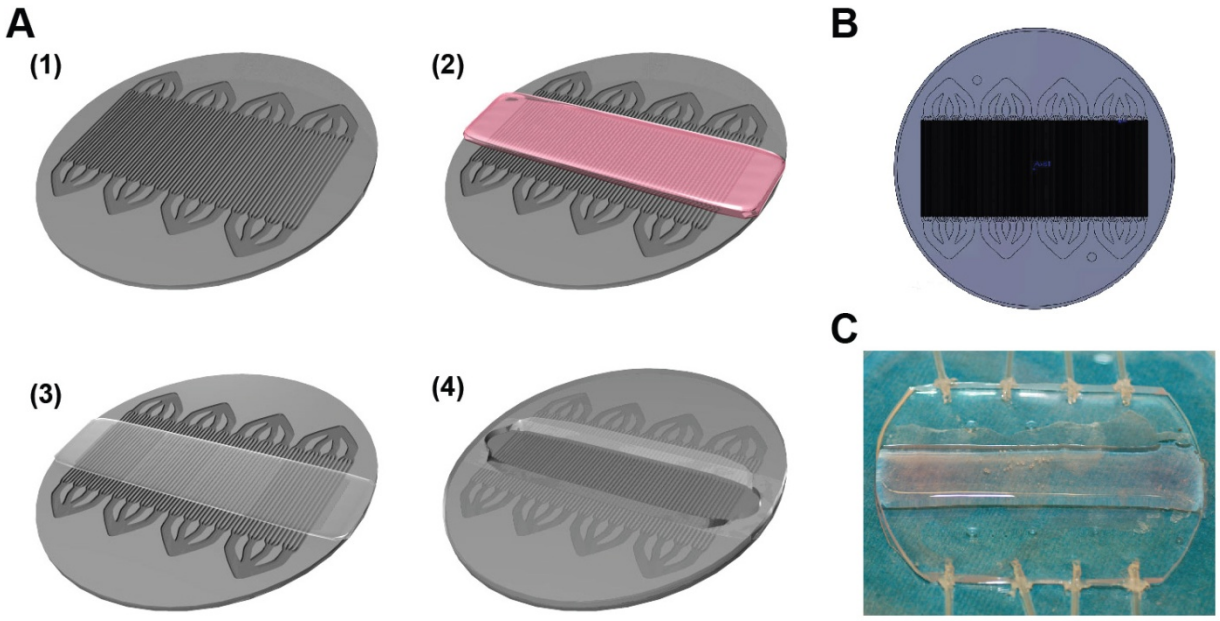

Figure 2-2. Manufacture of collagen-membrane straight-channel devices. **(A)** Step-by-step schematic of production (stills from animated video), showing (1) vascular channel layer, (2) addition of collagen gel, (3) removal of dye and dessication of collagen membrane, and (4) bonding of gas chamber layer over the membrane and channels. **(B)** Solidworks model depicting actual appearance of channels. **(C)** Photograph showing appearance of collagen gel right after placement and removal of the bounding box.

a beveled edge to the air chamber proper to increase media-holding capacity for cell culture without increasing the fixed gas exchange interface distance (**Fig. 2-2A-4**). Lids were cast from a 10-cm tissue culture dish lid.

Each device was divided into four “quads,” each with an independent blood input and output, operated separately and treated as independent samples. Within each quad, a series of 1:4, 1:4, and 1:6 channel branchings produced 96 100x100 μm square “capillaries.” The air chamber was oriented orthogonally to the direction of the blood flow, interfacing with the capillaries below *via* the collagen membrane.

Collagen films separating the capillaries and air chamber were produced using a modified protocol based on Vernon *et al*.[30] Rat collagen I (BD Biosciences) was diluted in 1x DMEM saturated with sodium bicarbonate, and pH was adjusted to 7.5 with NaOH. To spatially constrain the collagen membrane over the designated gas exchange region, a PDMS mask with

a rectangular slit (20 mm or 13 mm wide for the 10 mm and 3 mm air chambers, respectively) was overlaid atop the PDMS vascular layer, and the assembly was treated with oxygen plasma for 5 s at 100 W (Model PX-250, March Plasma Systems, Concord, CA). Following removal of the mask, edges of the vascular layer bounding the channels on either side were trimmed to prevent collagen spill-over along hydrophilic edges.

The collagen membrane was synthesized *in situ* over the vascular layer by pipetting the collagen solution onto the channel side of the device and allowing it to gel at 37 °C. The prior selective plasma treatment defined a fixed hydrophilic region on the vascular channels, allowing reproducible dimensions of these membranes. Salts and dye were extracted by submerging the device in distilled water, then the film was allowed to desiccate completely. During this process, the membrane becomes taut across the channels, forming the fourth wall of a closed rectangular channel rather than lining the bottom.

Finally, devices were assembled by bonding the air chamber layer atop the vascular layer *via* oxygen plasma activation for 10 s at 100 W. Air inlets on either side of the device, as well as four pairs of blood inlets and outlets, were generated by boring channels with a tissue biopsy punch and affixing silicone tubing with RTV silicone glue, with luer-lock fittings to interface with syringes for cell seeding and the gas exchange setup. All devices were sterilized by ethylene oxide prior to use.

2.4 Cell culture on multi-channel gas exchange devices:

Human umbilical vein endothelial cells (HUVECs) were cultured in EGM-2 media (Lonza) and then seeded into vascular channels at 2-5×10^6 cells/mL (~200 µL per quad). The air chamber was filled with EGM-2 media, and inverted devices were incubated in standard tissue culture conditions for 1 hour to promote attachment to the collagen membrane.

A549 cells were introduced into the upper chamber of the device at 1×10^5 cells/mL in a total of ~10 mL DMEM with 10% FBS, 100 U/mL penicillin, and 100 µg/mL streptomycin, then

the devices were subsequently incubated for several days in the upright orientation until both cell populations reached confluency. All media in the air chamber was drained and replaced with ambient air prior to gas exchange testing.

2.5 Gas exchange testing of multi-channel collagen-membrane devices

Whole sheep's blood was aliquoted into capped 60-mL syringes and incubated at 37 °C overnight to approximate gas content of venous blood in accordance with the guidelines for baseline blood parameters set forth in ISO 7199 for blood oxygenator testing.[31] Following incubation, the average baseline values were: SpO_2 70%; pCO_2: 48 mmHg (6.4 kPa); hemoglobin: 10.1 g/dL.

The experimental setup for gas exchange testing of multi-channel collagen-membrane devices is depicted in **Figure 3-3A** (page 18). 0.1 L/min of 100% oxygen was bubbled through a humidifying column, then introduced into the air chamber, flowing orthogonally over all vascular channels before exiting to ambient air. The ventilation rate was the lowest setting on the regulator and represents an excess of O_2, rather than a realistic $\dot{V}/Q$ ratio. The device was infused with blood using a syringe pump (PHD 2000, Harvard Apparatus), with the blood input flowing through gas-impermeable PVC tubing. Because of the thickness of the PDMS walls bounding the non-collagen sides of the channels, we calculated that the contribution of gas transmission through these walls to the total gas exchange is negligible. Tubing and devices were enclosed in an incubator to maintain the temperature at 37 °C (Hybaid HS9320, Fisher Scientific). Baseline measurements were drawn from a three-way valve immediately upstream of the device, while experimental measurements were taken from a valve connected to the output tubing, with no opportunity for further gas exchange after the blood exited the vascular bed. Blood gases, pH, hematocrit, and bicarbonate levels were measured immediately upon sample acquisition using a Stat Profile Critical Care Xpress 12 (Nova Biomedical).

2.6 Other Techniques

Transmission electron microscopy: Membranes were extracted from the devices and fixed in 2% glutaraldehyde. Imaging of cross-sections was performed by the PMB Microscopy Core at Massachusetts General Hospital.

Immunofluorescence: Following 2-3 days in culture, cells were stained *in situ* on the membranes using anti-CD31 antibody (clone TLD-3A12, Millipore) at 10 μg/mL, phalloidin (Alexa Fluor 568 phalloidin, Invitrogen), and Hoechst.

Data Analysis and Statistical Testing: Data were tabulated and analyzed in Excel (Microsoft Corp.), and statistical analysis and plotting was performed in GraphPad Prism (GraphPad Software, Inc.). For two-way ANOVA analysis in Figures 3-3 and 3-4, Bonferroni post-tests were conducted in two ways: first, comparing the four configurations against each other within each flow rate (significant differences are indicated in the figures, and all omitted relationships are non-significant), and second, comparing different flow rates against each other within each configuration (for clarity, these significant differences are *not* indicated in the figures, but are noted in the text).

3 Results

3.1 Gas exchange in proof-of-concept collagen-membrane transwell devices

We set out to design blood gas exchange devices centered on gas exchange across thin collagen membranes, hypothesizing that such membranes would not only recapitulate efficient gas exchange as seen in alveolar membranes, but also serve as a malleable substrate for relevant cell populations. As a demonstration of the feasibility of integrating cellularized collagen membranes into microfluidic devices for blood gas exchange, we first designed a prototype using a collagen membrane mounted on a transwell (**Fig. 3-1A**). We seeded human umbilical vein endothelial cells (HUVECs) and "parenchymal" cells (H441 lung adenocarcinoma cell line) on opposite sides of the membrane to mimic the sequence of cells found in the native alveolar blood-air interface (**Fig. 3-1B**). To examine whether such adherent cells may remodel the collagen substrate in the context of these devices *in vitro*, we compared the thicknesses of membranes in tissue-engineered alveoli when incubated with media alone versus cultured with HUVECs and H441 cells. After 14 days, we measured a statistically significant 31% reduction in collagen film thickness in the presence of cells (**Fig. 3-1C, left**), determined by TEM (**Fig. 3-1C, right**). To establish the practical impact of the presence of cells and change in film thickness, we affixed the tissue-engineered transwells on a single polydimethylsiloxane (PDMS) microfluidic channel such that the endothelial side directly formed the top of the channel and the parenchymal layer was in direct contact with air in the transwell chamber (**Fig. 3-1A**). We then measured oxygen exchange by flowing sheep's blood at 0.0625 mL/min through the vascular channel and pure oxygen at 0.1 L/min through the air chamber (**Fig. 3-1D**). pO_2 increases were comparable between the acellular collagen, endothelial cells-on-collagen, and fibroblasts-on-collagen controls, whereas seeding with both endothelial and "parenchymal" cells led to a statistically significant improvement in oxygenation. Together, these results established that thin collagen films can function as gas exchange membranes and support bifacial cell cultures, which in turn interact with and reconfigure the membrane.

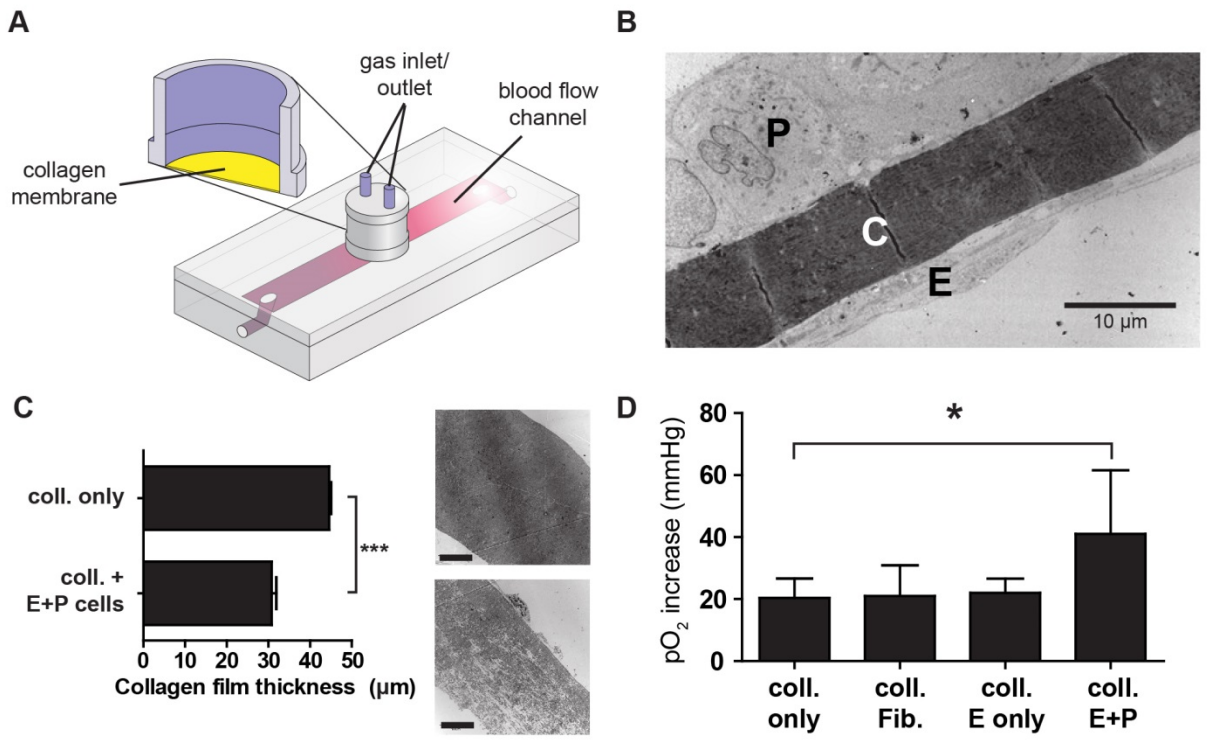

Figure 3-1. Performance of collagen-membrane transwell devices. (A) Schematic of single-channel transwell device with blown-up detail showing location of the collagen membrane; reproduced for reference from Figure 2-1. **(B)** TEM showing detail of collagen membrane [C] in tissue-engineered alveolus with H441 lung adenocarcinoma cell [P] and HUVEC [E]. **(C)** Change in collagen film thickness due to presence of attached endothelial cells and pneumocytes. *Inset:* TEM images of the membranes following incubation with either control medium without cells, top, or HUVECs and H441s, bottom. Scale bar = 10 μm. **(D)** Oxygenation of blood (measured as change in partial pressure of oxygen from inlet to outlet) via gas exchange across various membranes in the tissue engineered alveolus. coll. = collagen membrane; E only = endothelial cells only; E+P = endothelial cells (HUVECs) and pneumocytes (H441); Fib. = fibroblasts.

3.2 Acellular multi-channel collagen-membrane devices mediate efficient gas exchange

Based on these initial insights, we designed and manufactured multi-channel collagen-membrane gas exchange devices that would allow us to rigorously quantify the impact of membrane thickness, gas exposure length, and flow rate on gas exchange. The devices contained four independent PDMS vascular beds (“quads”), each comprised of a vascular tree branching into 96 parallel channels that interface with a common air chamber *via* a large, contiguous collagen membrane (**Figure 3-2A**). The geometric layout of channel branching and

cross-sectional dimensions were based on prior designs and modeling, in which vascular networks with physiologic hemodynamics and efficient gas transfer were tested in the context of lung assist devices that employed thin, acellular silicone membranes.[28] For our new collagen-membrane devices, we used channels with 100 × 100 μm square cross-sections, since in previous studies, larger channels (150 × 150 μm) were too deep to achieve full saturation during gas exchange, while shallower channels were less efficient due to lower throughput capacity.[28]

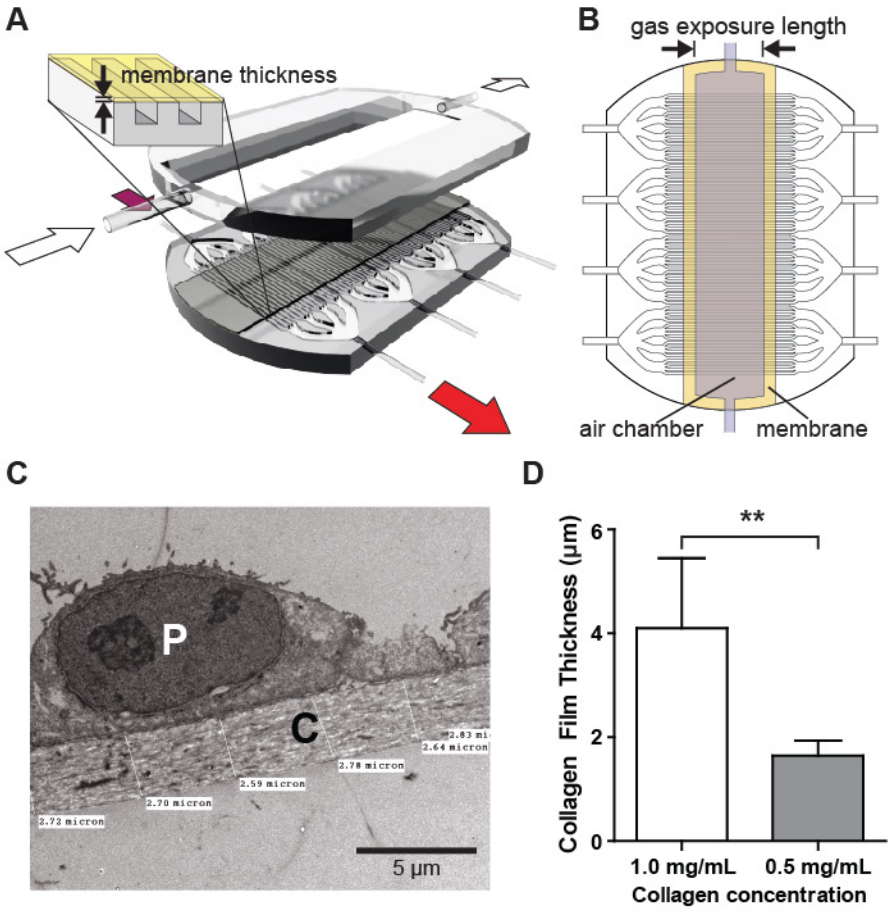

Figure 3-2. Properties of collagen membranes in multi-channel devices. (A) Three-dimensional schematic of a multi-channel collagen-membrane lung device, showing the assembly of the lower channel layer, collagen membrane, and parenchymal/gas chamber layer. Bloodflow is indicated by the dark arrows; airflow is indicated by the light arrows. Blown-up detail shows orientation of the collagen membrane and vascular channels (channels not to scale). **(B)** Overhead schematic of vascular channels with overlaid collagen membrane and air chamber to demonstrate alignment (channels not to scale). **(C)** TEM showing detail of collagen membrane [C] in tissue-engineered alveolus with A549 lung carcinoma cell [P]. **(D)** Comparison between thicknesses of collagen membranes produced using different collagen concentrations.

To explore the design space, we created device configurations with different gas exposure lengths at the fluid-air interface (3 mm vs. 10 mm, defined in **Fig 3-2B**) and different thicknesses of collagen membranes as governed by the concentration of collagen in the collagen gel prior to desiccation (1.0 vs. 0.5 mg/mL). The gas exposure lengths were calculated to allow for blood traversal times on the order of one second at flow rates of interest, roughly corresponding to lung capillary gas exposure durations.[32] Recognizing that the magnitude of oxygen transfer in the single-channel transwell prototype was fairly modest, and hypothesizing that this result could be in part due to the thickness of the collagen membrane, we aimed to synthesize collagen membranes approximately an order of magnitude thinner than in the transwells. As measured by TEM on cross-sections of several collagen membranes (**Fig 3-2C**), film thickness was proportional to the collagen concentration in the cases tested, with 1.0 and 0.5 mg/mL gels yielding ~4 μm and ~2 μm membranes, respectively (**Fig 3-2D**). These selected thicknesses were approximately informed by the human alveolus, where the gas exchange membranes are ~0.4-2 μm thick.[32, 33]

We tested the gas exchange capacity of these acellular collagen-membrane devices using the experimental assembly depicted in **Figure 3-3A**: whole blood with typical venous oxygen and carbon dioxide content (average SpO_2: 70%, pCO_2: 48 mmHg) was pumped steadily into the devices' channels at flow rates of 0.0528, 0.1584, 0.3168, or 0.528 mL/min/quad while humidified oxygen flowed through the air chamber at a rate such that the oxygen concentration would not be meaningfully affected by gas exchange. The blood flow rates were determined based on approximate normal physiologic limits of shear stress, with the highest flow rate corresponding to 50 dyn/cm^2, a figure based on the range of shear stresses experienced by endothelial cells in human arteries and far below the shear limit of erythrocytes.[34, 35] The flow rate to shear stress correspondence and the number of quads tested for each physical configuration at these blood flow rates are recorded in **Table 3-1**. For each condition, we

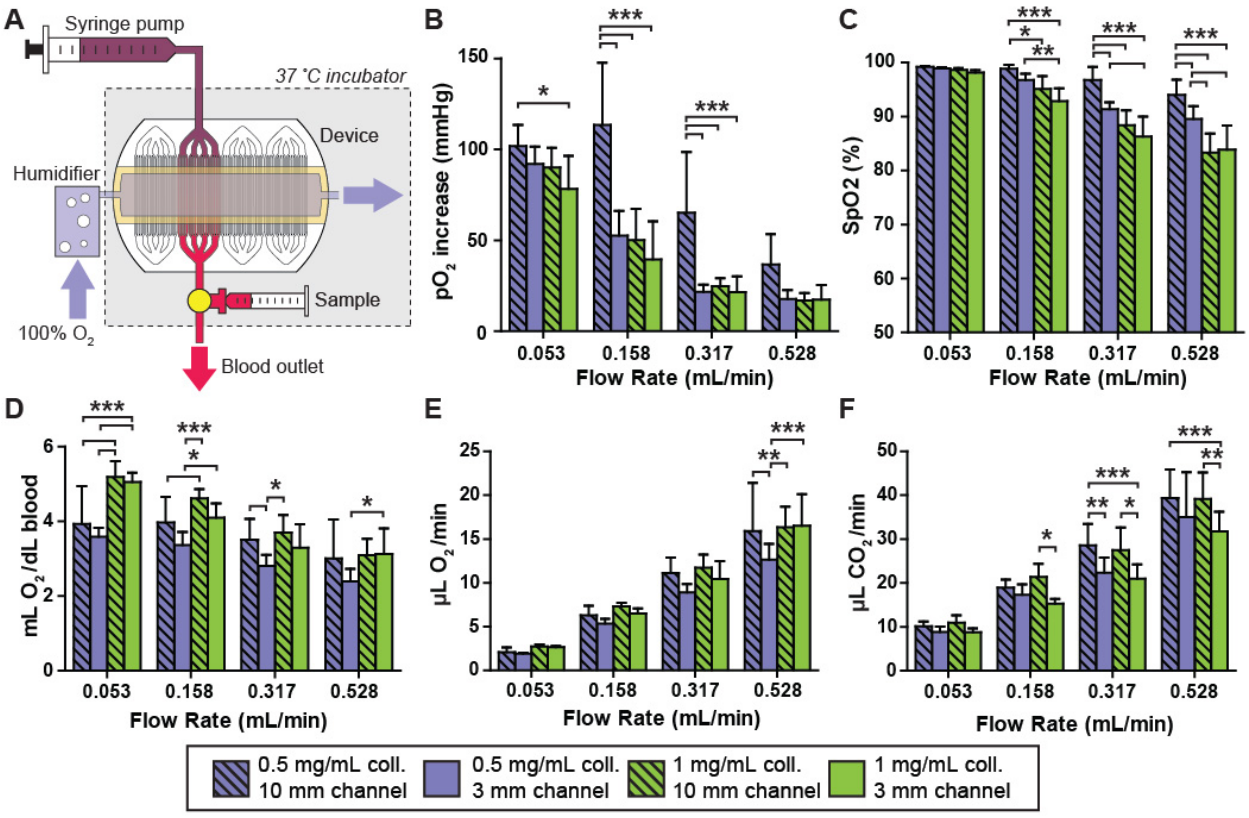

Figure 3-3. Gas exchange in acellular multi-channel collagen-membrane devices. (A) Schematic representation of the gas exchange setup for testing both acellular and cellularized straight-channel devices. **(B)** Oxygenation as a function of flow rate, membrane thickness, and channel length, as measured by increase in partial pressure of oxygen. For panels **B-F**, *: $p < 0.05$, **: $p < 0.01$, ***: $p < 0.001$ by two-way ANOVA with Bonferroni post-test comparing configurations within each group. **(C)** Hemoglobin oxygen saturation (%) as a function of flow rate, membrane thickness, and channel length. **(D)** Oxygen transfer per deciliter of blood. **(E)** Oxygen transfer per unit time. **(F)** Carbon dioxide clearance per unit time.

	0.0528	0.158	0.317	0.528	Flow rate (mL/min/quad)
	5	15	30	50	Shear stress (dyn/cm^2)
1 mg/mL, 3 mm	9	9	9	9	
1 mg/mL, 10 mm	6	6	6	6	
0.5 mg/mL, 3 mm	10	10	10	10	
0.5 mg/mL, 10 mm	11	11	10	9	

Table 3-1. Number of quads tested at each set of parameters (blood flow rate, collagen membrane concentration, and gas exposure length)

measured the partial pressures of oxygen (pO_2) and carbon dioxide (pCO_2), oxygen saturation (SpO_2), bicarbonate, total CO_2, hemoglobin concentration, and pH.

The 0.5 mg/mL membrane / 10 mm exposure length quads showed significantly larger increases in oxygen tension compared to the other three conditions in two of the flow rates tested ($p < 0.001$ by two-way ANOVA with Bonferroni post-test comparing configurations within each flow rate) (**Figure 3-3B**). Additionally, all device configurations trended towards greater increases in pO_2 with slower flow rates.

Because the principal contributor to oxygen content in blood is the level of hemoglobin oxygen saturation, rather than freely dissolved oxygen, we also compared the configurations in terms of the oxygen saturation of blood exiting the device, drawn directly from gas-impermeable tubing at the device's outlets to preclude extraneous contact between the blood and ambient air. At the most rapid flow rate, saturation was lowest in the two thicker membrane conditions and highest in the 0.5 mg/mL membrane / 10 mm exposure length configuration, in keeping with intuition (**Figure 3-3C**). Overall, regardless of membrane parameters, complete oxygen saturation (99-100%) was observed at the slowest flow rate while increases in flow rate led to diminishing saturation.

To integrate the hemoglobin-bound and dissolved oxygen measurements, the total oxygen content (mL O_2/dL blood) was computed from the following formula:[36]

$$O_2\ content = 1.34\ \left(\frac{mL\ O_2}{g}\right) \times \mathrm{Hgb}\ \left(\frac{g}{dL}\right) \times SpO_2 + 0.003\,\frac{mL}{mmHg} \times pO_2(mmHg)$$

As anticipated, the oxygen content of the exiting blood showed similar trends to the oxygen saturation (**Figure 3-3D**). The total oxygen transfer rate (mL/min) was then calculated from these values and the blood flow rate as follows:

$$O_2\ transfer\ rate = Flow\ rate \times (output\ blood\ O_2\ content - baseline\ blood\ O_2\ content)$$

This metric, which quantified the functional efficiency of the device, revealed the significant impact of increasing blood throughput on the overall gas-exchange capacity of the collagen-membrane lung devices (**Fig. 3-3E**). The oxygen transfer normalized to total membrane surface area, including collagen spanning inter-channel walls, ranged from 33-46 mL/min/m^2 at the minimal flow rate of 0.0528 mL/min to 220-288 mL/min/m^2 at the maximal flow rate of 0.528 mL/min. In addition to oxygen-related parameters, we also measured the changes in partial pressure of carbon dioxide (pCO_2), plasma bicarbonate, and total CO_2 in the same samples. The carbon dioxide clearance per unit time displayed the same trends as oxygenation but with higher magnitude across-the-board, in accordance with the higher rate of diffusion of carbon dioxide versus oxygen (**Fig. 3-3F**). The carbon dioxide transfer ranged from 153-190 mL/min/m^2 at the minimal flow rate of 0.0528 mL/min to 553-685 mL/min/m^2 at the maximal flow rate of 0.528 mL/min.

3.3 Collagen-membrane lung devices support cell culture while maintaining function

While acellular collagen-membrane lung devices represent an important step towards biomimetic design, the incorporation of cellular components is an important step towards future goals of both avoiding thrombogenicity as well as maintaining the integrity of the collagen membrane in the long-term. Analogously to the single-channel transwell devices, we cultured endothelial cells (HUVECs) and “parenchymal” cells (A549) on opposite sides of the collagen membrane, facing the vascular channels and air chamber, respectively. We confirmed the presence of both cell types *via* immunofluorescent staining for CD31 (endothelial cell junctions) and F-actin (any cell cytoplasm) as shown in **Figure 3-4A**, which depicts a partially-confluent cellularized collagen membrane during the culture process; a confluent parenchymal cell layer is shown in **Fig. 3-5A**. To ensure that cells would not be dislodged by the presence of flow in the channels, we seeded endothelial cells in the device channels as before; after they had adhered, we subjected them to media flowing at 0.5 mL/min/quad for a period of 3 hours, confirming

through immunofluorescence that the endothelial layer remains intact on the collagen membrane (**Fig. 3-5B**).

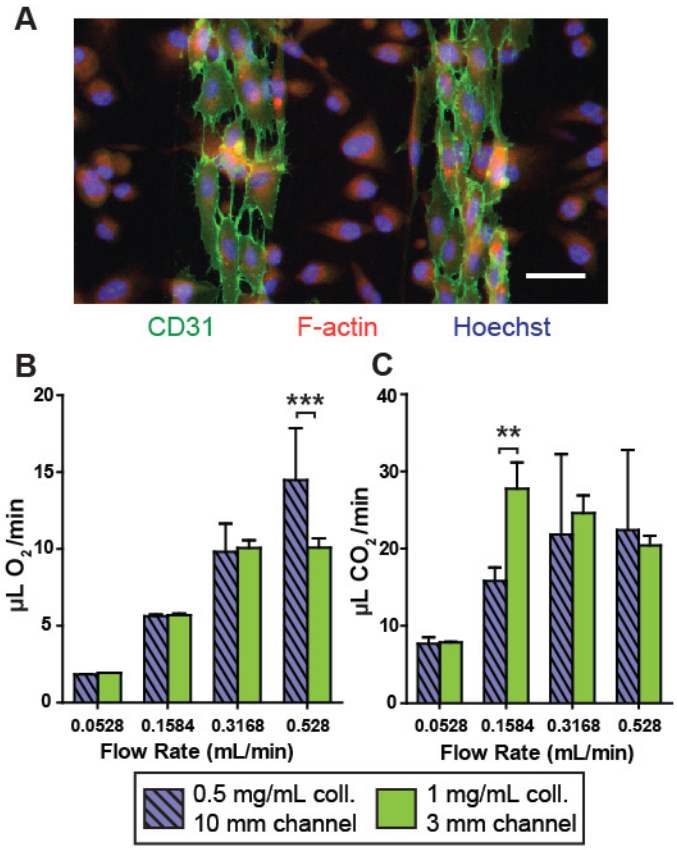

Figure 3-4. Gas exchange in cellularized multi-channel collagen-membrane devices. (A) Immunocytochemical stain showing co-culture of endothelial cells and lung epithelial cells, partway through the culturing process. Green: CD31; red: F-actin; blue: nuclei. Scale bar: 50 µm. **(B)** Oxygen transfer per unit time in devices cultured with HUV endothelial cells in the channels and A549 parenchymal cells in the gas chamber. For **B** and **C**, *: $p < 0.05$, **: $p < 0.01$, ***: $p < 0.001$ by two-way ANOVA with Bonferroni post-test comparing configurations within each group **(C)** Carbon dioxide clearance per unit time in devices with cell co-culture.

We then performed gas exchange testing on two of the original four configurations as cellular devices: 1 mg/mL collagen with 3 mm channel length (n=5) and 0.5 mg/mL collagen with 10 mm channel length (n=3). The rates of oxygen and carbon dioxide transfer in cellularized devices (**Fig. 3-4 B-C**) were comparable to those in acellular devices, but notably, the oxygenation was not significantly different between the two fastest flow rates, and carbon dioxide release was not significantly different among the three highest flow rates.

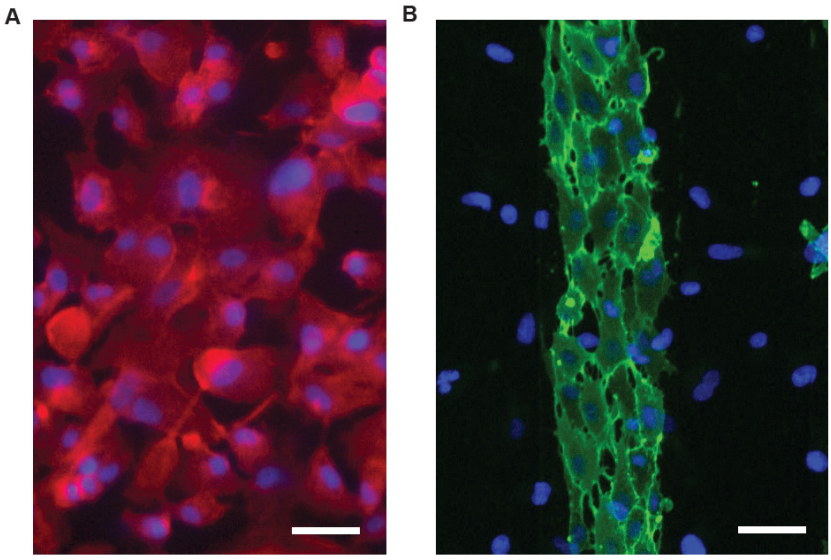

Figure 3-5. Cell culture on collagen membranes. (A) A549 cells forming nearly confluent layer on the parenchymal side of the collagen membrane. Red: Phalloidin; Blue: Nuclei (Hoechst). Scale bar: 50 μm **(B)** HUVECs adhered to collagen membrane after device has been subjected to media flow at 0.5 mL/min for 3 hours. Green: CD31; Nuclei (Hoechst). Scale bar: 50 μm

4 Discussion

Our results establish the feasibility of using ultra-thin collagen membranes in gas exchange devices. The type I collagen membranes that we tested were easily colonized by endothelial and epithelial cells in a configuration mimicking the native alveolus, demonstrated by the bifacial seeding of representative cell populations in the tissue-engineered alveolus devices (**Fig. 3-1B**). Moreover, these membranes were extensively remodeled by adherent cells, producing thinner membranes (**Fig. 3-1C**). In our multi-channel devices, the membranes were as thin as 2 μm, approaching the normal range of the human alveolar-capillary barrier (~0.4-2 μm). Furthermore, the generalized method of producing such membranes could be easily tailored to test varying compositions of extracellular matrix in the future to support cell attachment and differentiation.

The key metric of performance for any artificial lung device is gas exchange: blood oxygenation and carbon dioxide clearance. At the highest flow rate, the acellular multi-channel devices exhibited excellent oxygen exchange efficiency: up to 16.5 μL O_2/min on a surface area of 57.5 mm^2 per quad (including “dead” membrane spanning PDMS supports). This corresponds to a gas transfer efficiency of 288 mL/min/m^2, or 574 mL/min/m^2 when considering only the collagen membrane in contact with blood. This compares favorably against the previous generation of lung devices from our lab, which achieved 34 mL/min/m^2,[37] and approaches the native human lung, which transfers oxygen at 21-65 mL/min per mmHg of oxygen gradient[38] over a ~70 m^2 surface area, for an efficiency of approximately 217-672 mL/min/m^2 on pure oxygen. Because the output oxygen saturation – and thus total oxygen transferred per deciliter of blood – was only moderately decreased by the flow rate, the oxygen transfer rate per unit time always increased with increasing blood flow rates (**Fig. 3-3E**). For these studies, we capped flow rates at physiologic arterial shear stresses, but it is likely that an endothelial cell layer would allow higher flow rates that could correspond to further increases in oxygen transfer. Furthermore, noting that the maximal gas transfer rate in the 1 mg/mL membrane devices was

essentially equal for the 3 mm and 10 mm channel lengths (16.5 and 16.4 μL O_2/min, respectively), it is likely that greater efficiency per unit area may be achieved by further shortening the channel length towards the physiologic order of magnitude, as our group has tested in silicone-membrane devices down to 0.3 mm.[28]

Although the oxygen transfer in these devices was excellent, we observed scenarios in which the output blood was not fully saturated and the pO_2 did not reach the ideal of at least 100 mmHg, reflecting the net influence of channel depth, membrane properties, flow rate on the devices' performance. In the acellular collagen-membrane devices, we observed a general trend towards greater increases in ΔpO_2 at slower flow rates, regardless of collagen membrane thickness or residence time, ranging from ~20 mmHg at 0.528 mL/min/quad to ~100 mmHg at 0.0528 mL/min/quad (**Fig. 3-3B**). The configuration with the thinnest membrane and longest gas exposure distance showed the greatest magnitude of ΔpO_2 at all flow rates, with statistically significant differences versus the other configurations at all but the fastest blood flow rate. This result agrees with the hypothesized impact of thinning the membrane or lengthening the channel length and argues for the importance of working with ultra-thin collagen membranes that approach the thickness of the alveolar gas exchange barrier.

At the highest flow rates tested in our study, the blood output reached oxygen saturations in the 80-95% range rather than full saturation (**Fig. 3-3C**), suggesting that there is still room for device optimization. As with the ΔpO_2 data, the effect was most pronounced with the thicker membrane and shorter gas exposure distance conditions, but in all configurations, the oxygen saturation at the 0.0528 mL/min flow rate was statistically significantly better than the saturation at the 0.528 mL/min flow rate ($p < 0.001$ by two-way ANOVA with Bonferroni post-test comparing across flow rates). One strategy for addressing incomplete saturation without further thinning the membrane or lengthening the channel is to reduce the channel size: We have previously shown in silicone-membrane devices that if the channel size is decreased below 100 μm, the oxygen saturation improves at a given residence time of blood in contact with air, with

the drawback being lower overall blood flow rates.[28] As such, one contributing factor to the incomplete hemoglobin saturation at faster flow rates may be the laminar flow in these straight, narrow, 1:1 aspect ratio channels, where minimal mixing is preferable for reducing the risk of thrombus formation but less amenable to facilitating gas exchange. The optimal channel size is not yet understood but must balance (1) achieving optimal hemoglobin saturation, (2) allowing ample blood flow rate so that a device with practical oxygenation capacity remains a reasonable size, and (3) minimizing the risk of thrombus formation. Since the risk of thrombosis is dependent on both physical factors (channel size, flow rate) and biological factors (wall coatings, endothelialization, anticoagulation), the optimal size will depend on the success of incorporating biocompatible elements such as endothelialization. In this work, endothelial cells adhered to only the face of the channel comprising the membrane; ideally, endothelialization would be present on all sides of the channel. Such complete coating could be enabled by alternate collagen deposition techniques to complement our current process, which due to contraction during the drying process lifts the membrane over rather than lining the PDMS channels. Without complete endothelialization, it may not be possible to reduce the channel size much farther than the current ~100 μm range, whereas complete endothelialization may permit reduction of the channel diameter close to the native lung capillaries at around one red cell width (~10 μm). Very small channels, which promote greater gas exchange surface per cross-sectional area of the channel, do come at the cost of requiring additional scaffolding to move blood at a given overall rate; therefore, the ideal channel size will probably lie between these two orders of magnitude.

Despite observations of incomplete oxygen saturation, the data overall remain most consistent with the oxygenation process being blood perfusion-limited rather than oxygen diffusion-limited, similar to the situation in native lungs, which are only diffusion-limited in the case of extreme physical exertion or diseased states.[32] While diffusion-limited devices would be expected to show approximately constant oxygen transfer rates at all flow rates, with oxygen

transfer per unit volume of blood dropping off as flow rates increase, the multi-channel collagen-membrane devices instead showed increasing oxygen transfer rates (**Fig. 3-3E**) and fairly steady oxygen transfer per unit volume (**Fig. 3-3D**) with increasing flow rate. Indeed, over the flow rates tested, the oxygen transfer rate (**Fig. 3-3E**) as a function of perfusion can be closely approximated with linear regression through the origin, with R^2 of 0.92-0.97 for all configurations. In the future, greater oxygen transfer efficiency may be achieved by further increasing flow rates, limited only by the shear tolerance of endothelial cells.

In addition to blood oxygenation, carbon dioxide clearance from blood is also centrally important for lung devices. The trends in carbon dioxide transfer mirrored those in oxygen transfer, with absolute volumes about twice as large (**Fig. 3-3F**). The carbon dioxide clearance is adequate to lower pCO_2 into the normocapnic range, even at the highest flow rates (from a baseline of ~50 mmHg to <40 mmHg in the acellular devices). In keeping with the efficient O_2 gas transfer on a per-area basis, the maximal CO_2 transfer achieved with the collagen membrane devices was 685 mL/min/m^2. These higher CO_2 transfer rates are similar to what we have observed with silicone membranes in a microchannel- based lung device[37] and are consistent with the native lung, which also exhibits higher maximal CO_2 transfer rates.

The cellularized devices yielded similar magnitudes of oxygen and carbon dioxide transfer per minute compared to the acellular devices, peaking at around 10 μL/min O_2 and 20 μL/min CO_2 (**Fig. 3-4 B-C**). Interestingly, there were not significant differences between the two highest blood flow rates for oxygen transfer in either cellularized configuration, implying diffusion limitation in this regime. The diffusion limitation may be related to the membrane and associated cells, diffusion through the entire depth of the channel, or likely a combination of both. This finding may also reflect the limitations of our model cell lines, as the inherent thickness of A549 cells compared to healthy primary pneumocytes may impede effective gas exchange as compared to the bare membrane or a membrane lined with flat epithelium. It is thus possible that use of more phenotypically stable, differentiable cells such as neonatal lung epithelial cells

or iPS-derived alveolar epithelial cells may reconcile the cellular device data with the acellular data.

The blood gas exchange results for cellularized devices serve as a first step towards harnessing the potential of cellularization to improve long-term durability of collagen membranes and reduce thrombogenicity. Experiments relating to these hypotheses (such as long-term perfusion followed by imaging of thrombus deposition, platelet adhesion studies, and staining to assess endothelial cell activation state) could not be tested in the current device design, since the present membrane only comprises one of the four walls of the square channels. As such, comparisons to existing technologies regarding durability and biocompatibility cannot be made at this time. However, alternative methods of collagen patterning and deposition could produce channels wholly comprised of collagen, enabling future blood biocompatibility studies; furthermore, long-term durability may be tested with differentiated cells that would not overgrow after reaching a confluent layer.

5 Conclusions, Future Directions, and Perspectives

In summary, we have designed and tested collagen membrane-based lung assist device prototypes that exhibit favorable oxygen and carbon dioxide exchange capacity. The membrane readily supports adherent endothelial and parenchymal cells, which are able to remodel the membrane.

Much work obviously remains, both in the form of innovations to create fully endothelialized channels, as well as optimization to minimize the overall size of the device to enable large-scale, modular construction and accommodate clinically-relevant total blood flow rates. Towards the former, groups have shown that collagen and other extracellular matrix adhesion molecules may be patterned *via* chemical vapor deposition (CVD),[39] which would allow coating of the inner walls of channels in a complementary manner to our collagen gels that create the "floating" upper wall. Alternatively, channels may be constructed of sacrificial material within collagen gels, such that removal of this sacrificial material opens up channels that may then be seeded with endothelial cells.[40] These and other technologies (such as novel tissue adhesives[41]) could potentially create fully endothelialized channels, which would enable testing of key biocompatibility properties such as endothelial surface marker expression and activation of the coagulation cascade when fresh, non-anticoagulated blood is used.

Regarding the latter issue of modular construction, the eventual required scale in a human being would be 500-5000 mL/min of total bloodflow, depending on application: the lower end for CO_2 removal; the upper end for full oxygenation and cardiac support. The current devices are not optimized for space; even so, the relevant vascular bed for the 100 μm channels, for instance, occupies an approximate volume of 57.5 mm^2 surface area (membrane-exposed channel only) x 200 μm (accounting for equal separation below the channels as between them horizontally), which comes out to 11.5 mm^3 for a flowrate of 0.528 mL/min. In this case, 5000 mL/min would occupy ~110 cm^3 (approximately a cube 5 cm to the side) for the vascular elements, without accounting for air channels. The additional structures for air

channels and vascular branching will obviously add volume, but it is encouraging that this preliminary figure is in a reasonable order of magnitude. The straightforward parallel-channel architecture contrasts sharply with the native human alveolus, but has the advantages of being easy to manufacture – less prone to defects – and spatially efficient. Indeed, the cross-current architecture that we employ is reminiscent of the structure of the avian lung, which is regarded as more efficient than the human lung.[42] For the architecture of channels leading up to the respiratory capillaries, prior work in our group has informed general design principles that can guide branching geometries to maximize biocompatibility.[34]

Since the time when the experiments presented here were performed (*c.* 2008-2009), immense progress has been made in the capacity to derive key cell phenotypes to populate tissue-engineered lung assist devices. Because of the hybrid approach in our work, combining PDMS with collagen and cells, the number of cell types required is greatly reduced: the essentials would be Type I alveolar cells and respiratory endothelial cells. Because there is no equivalent of lung inflation, surfactant is not required to prevent airway collapse (though Type II cells are needed for renewal of Type I cells). Further, the absence of large airways and true arteries eliminates the need for ciliated cells (air filters would suffice in their stead), smooth muscle cells (vessel “tone” can be maintained with the PDMS scaffolding), and chondrocytes (again replaced by PDMS). At present, primary microvascular endothelial cells may be cultured and expanded *in vitro* from a biopsy sample or similar, and pneumocytes or their precursors may be generated from donor-derived adult or induced pluripotent stem cells. Use of these cell types would be an important step forward from the proof-of-concept cell lines used in our studies here.

Overall, combining artificial oxygenator technology with biological elements such as ECM and cells is an appealing approach for creating hybrid devices with predictable, tunable properties while reducing exposure to foreign material compared to ECMO. We ultimately envision that incorporation of biologically-inspired gas exchange interfaces, in conjunction with

advancements in microfluidic device design, may ultimately yield efficient, biocompatible lung devices that can supplement native lungs in patients with chronic lung disease.

6 Appendix: List of Abbreviations and Acronyms

aPTT: Activated partial thromboplastin time

ARDS: Acute respiratory distress syndrome

COPD: Chronic obstructive pulmonary disease

DMEM: Dulbecco's modified Eagle medium

$ECCO_2R$: Extracorporeal carbon dioxide removal

ECMO: Extracorporeal membrane oxygenation

ECM: Extracellular matrix

EGM: Endothelial growth media

ESC: Embryonic stem cell

HUVEC: Human umbilical vein endothelial cell

iPSC: Induced pluripotent stem cell

PDMS: Poly(dimethylsiloxane)

7 Acknowledgments

I would like to thank Dr. Joseph Vacanti and Dr. David Hoganson for their mentorship on this project and beyond. I could not imagine having a more exciting and rewarding research experience as a first-year medical student! Thanks to Erik Bassett for sharing his mechanical engineering expertise and project experience with me. I am grateful for the support of all the other lab members, particularly PIs Dr. Cathryn Sundback, Dr. Craig Neville, and Dr. Irina Pomerantseva, for their guidance and help in getting me quickly on my feet in the lab; and all the medical students, post-docs, technicians, and high school students (Elliot Penson and Amita Gupta, who provided immense help –they've both since graduated from college!). Jacqueline Ferraro-Pipes has helped immensely on the administrative side of things, especially with publishing this work and preparing this thesis in the years after I left the lab.

For the experiments, we could not have gathered the key results without the help of Baoling Liu, Yongqing Li, *et al*. who lent us their blood gas analyzer and lab space; Mary McKee at the PMB Microscopy Core at Massachusetts General Hospital who took the TEM images; and Jessica Melin and the Stanford Microfluidics Foundry who manufactured the microfluidic molds.

I would also like to thank my MD advisor, Dr. Lee Gehrke, MD-PhD advisor, Dr. David Frank, and HST advisor, Dr. Richard Mitchell, for all their guidance and expertise. And last but not least, I need to thank my HMS/HST/MD-PhD colleagues, friends, and family for their support and great ideas.

I gratefully acknowledge financial support from the NIH/NIGMS as part of the Medical Scientist Training Program at Harvard Medical School (T32GM007753).

8 References

The key results presented in this thesis have been published in the following article:

J.H. Lo, E.K. Bassett, E.J. Penson, D.M. Hoganson, and J.P. Vacanti. Gas transfer in cellularized collagen-membrane lung assist devices, *Tissue Engineering Part A*. 2015 Jul 16.

Additional details regarding the vascular network architecture in the context of ultra-thin silicone membranes may be found in the following earlier publication from the Vacanti lab:

E.K. Bassett, D.M. Hoganson, **J.H. Lo**, E.J. Penson, and J.P. Vacanti. Influence of vascular network design on gas transfer in lung assist device technology, *ASAIO J*, 57 (2011) 533-538.

---

[1] KD Kochanek, SL Murphy, J Xu, and B Tejada-Vera. Deaths: Final data for 2014. *Natl Vital Stat Rep*, 65 (2016) 1-122.

[2] BD Kozower, BF Meyers, MA Smith, NC De Oliveira, SD Cassivi, TJ Guthrie, H Wang, BJ Ryan, et al. The impact of the lung allocation score on short-term transplantation outcomes: A multicenter study. *J Thorac Cardiovasc Surg*, 135 (2008) 166-171.

[3] M Valapour, MA Skeans, JM Smith, LB Edwards, WS Cherikh, K Uccellini, AK Israni, JJ Snyder, et al. Optn/srtr 2015 annual data report: Lung. *Am J Transplant*, 17 Suppl 1 (2017) 357-424.

[4] S Fischer, MM Hoeper, S Tomaszek, A Simon, J Gottlieb, T Welte, A Haverich, and M Strueber. Bridge to lung transplantation with the extracorporeal membrane ventilator novalung in the veno-venous mode: The initial hannover experience. *ASAIO J*, 53 (2007) 168-170.

[5] MC Sklar, E Sy, L Lequier, E Fan, and HD Kanji. Anticoagulation practices during venovenous extracorporeal membrane oxygenation for respiratory failure. A systematic review. *Ann Am Thorac Soc*, 13 (2016) 2242-2250.

[6] M Mazzeffi, J Greenwood, K Tanaka, J Menaker, R Rector, D Herr, Z Kon, J Lee, et al. Bleeding, transfusion, and mortality on extracorporeal life support: Ecls working group on thrombosis and hemostasis. *Ann Thorac Surg*, 101 (2016) 682-689.

[7] FJ Mateen, R Muralidharan, RT Shinohara, JE Parisi, GJ Schears, and EF Wijdicks. Neurological injury in adults treated with extracorporeal membrane oxygenation. *Arch Neurol*, 68 (2011) 1543-1549.

[8] RR Thiagarajan, RP Barbaro, PT Rycus, DM McMullan, SA Conrad, JD Fortenberry, ML Paden, and Em centers. Extracorporeal life support organization registry international report 2016. *ASAIO J*, 63 (2017) 60-67.

[9] W Bartosik, JJ Egan, and AE Wood. The novalung interventional lung assist as bridge to lung transplantation for self-ventilating patients - initial experience. *Interact Cardiovasc Thorac Surg*, 13 (2011) 198-200.

[10] LW Lund and WJ Federspiel. Removing extra co2 in copd patients. *Curr Respir Care Rep*, 2 (2013) 131-138.

[11] CA Bermudez, D Zaldonis, MH Fan, JM Pilewski, and MM Crespo. Prolonged use of the hemolung respiratory assist system as a bridge to redo lung transplantation. *Ann Thorac Surg*, 100 (2015) 2330-2333.

[12] TC Page, WR Light, and JD Hellums. Oxygen transport in 10 microns artificial capillaries. *Adv Exp Med Biol*, 471 (1999) 715-721.

[13] JK Lee, MC Kung, HH Kung, and LF Mockros. Microchannel technologies for artificial lungs: (3) open rectangular channels. *ASAIO J*, 54 (2008) 390-395.

[14] JK Lee, HH Kung, and LF Mockros. Microchannel technologies for artificial lungs: (1) theory. *ASAIO J*, 54 (2008) 372-382.

[15] D Huh, BD Matthews, A Mammoto, M Montoya-Zavala, HY Hsin, and DE Ingber. Reconstituting organ-level lung functions on a chip. *Science*, 328 (2010) 1662-1668.

[16] D Huh, DC Leslie, BD Matthews, JP Fraser, S Jurek, GA Hamilton, KS Thorneloe, MA McAlexander, et al. A human disease model of drug toxicity-induced pulmonary edema in a lung-on-a-chip microdevice. *Sci Transl Med*, 4 (2012) 159ra147.

[17] KH Benam, R Villenave, C Lucchesi, A Varone, C Hubeau, HH Lee, SE Alves, M Salmon, et al. Small airway-on-a-chip enables analysis of human lung inflammation and drug responses in vitro. *Nat Methods*, 13 (2016) 151-157.

[18] T Kniazeva, AA Epshteyn, JC Hsiao, ES Kim, VB Kolachalama, JL Charest, and JT Borenstein. Performance and scaling effects in a multilayer microfluidic extracorporeal lung oxygenation device. *Lab Chip*, 12 (2012) 1686-1695.

[19] HC Ott, B Clippinger, C Conrad, C Schuetz, I Pomerantseva, L Ikonomou, D Kotton, and JP Vacanti. Regeneration and orthotopic transplantation of a bioartificial lung. *Nat Med*, 16 (2010) 927-933.

[20] TH Petersen, EA Calle, L Zhao, EJ Lee, L Gui, MB Raredon, K Gavrilov, T Yi, et al. Tissue-engineered lungs for in vivo implantation. *Science*, 329 (2010) 538-541.

[21] WJ Zhang, QX Lin, Y Zhang, CT Liu, LY Qiu, HB Wang, YM Wang, CM Duan, et al. The reconstruction of lung alveolus-like structure in collagen-matrigel/microcapsules scaffolds in vitro. *J Cell Mol Med*, 15 (2011) 1878-1886.

[22] H Sugihara, S Toda, S Miyabara, C Fujiyama, and N Yonemitsu. Reconstruction of alveolus-like structure from alveolar type II epithelial cells in three-dimensional collagen gel matrix culture. *Am J Pathol*, 142 (1993) 783-792.

[23] RW Bonvillain, S Danchuk, DE Sullivan, AM Betancourt, JA Semon, ME Eagle, JP Mayeux, AN Gregory, et al. A nonhuman primate model of lung regeneration: Detergent-mediated decellularization and initial in vitro recellularization with mesenchymal stem cells. *Tissue Eng Part A*, 18 (2012) 2437-2452.

[24] SX Huang, MD Green, AT de Carvalho, M Mumau, YW Chen, SL D'Souza, and HW Snoeck. The in vitro generation of lung and airway progenitor cells from human pluripotent stem cells. *Nat Protoc*, 10 (2015) 413-425.

[25] BR Dye, PH Dedhia, AJ Miller, MS Nagy, ES White, LD Shea, and JR Spence. A bioengineered niche promotes in vivo engraftment and maturation of pluripotent stem cell derived human lung organoids. *Elife*, 5 (2016).

[26] SE Gilpin, JM Charest, X Ren, LF Tapias, T Wu, D Evangelista-Leite, DJ Mathisen, and HC Ott. Regenerative potential of human airway stem cells in lung epithelial engineering. *Biomaterials*, 108 (2016) 111-119.

[27] KC Stone, RR Mercer, P Gehr, B Stockstill, and JD Crapo. Allometric relationships of cell numbers and size in the mammalian lung. *Am J Respir Cell Mol Biol*, 6 (1992) 235-243.

[28] EK Bassett, DM Hoganson, JH Lo, EJ Penson, and JP Vacanti. Influence of vascular network design on gas transfer in lung assist device technology. *ASAIO J*, 57 (2011) 533-538.

[29] C Hess, B Wiegmann, AN Maurer, P Fischer, L Moller, U Martin, A Hilfiker, A Haverich, et al. Reduced thrombocyte adhesion to endothelialized poly 4-methyl-1-pentene gas exchange membranes-a first step toward bioartificial lung development. *Tissue Eng Part A*, 16 (2010) 3043-3053.

[30] RB Vernon, MD Gooden, SL Lara, and TN Wight. Native fibrillar collagen membranes of micron-scale and submicron thicknesses for cell support and perfusion. *Biomaterials*, 26 (2005) 1109-1117.

[31] ISO. Iso 7199: Cardiovascular implants and artificial organs - blood-gas exchangers (oxygenators). ISO, Geneva, Switzerland, 2009.

[32] BM Koeppen and BAE Stanton. Berne & levy physiology, 6th ed. Mosby Elsevier, 2008.

[33] JN Maina and JB West. Thin and strong! The bioengineering dilemma in the structural and functional design of the blood-gas barrier. *Physiol Rev*, 85 (2005) 811-844.

[34] DM Hoganson, HI Pryor, 2nd, ID Spool, OH Burns, JR Gilmore, and JP Vacanti. Principles of biomimetic vascular network design applied to a tissue-engineered liver scaffold. *Tissue Eng Part A*, 16 (2010) 1469-1477.

[35] AJ Pappano and WG Wier. Cardiovascular physiology, 10th ed. Mosby, 2012.

[36] T Shimono, Y Shomura, I Hioki, A Shimamoto, H Tenpaku, Y Maze, K Onoda, M Takao, et al. Silicone-coated polypropylene hollow-fiber oxygenator: Experimental evaluation and preliminary clinical use. *Ann Thorac Surg*, 63 (1997) 1730-1736.

[37] DM Hoganson, HI Pryor, 2nd, EK Bassett, ID Spool, and JP Vacanti. Lung assist device technology with physiologic blood flow developed on a tissue engineered scaffold platform. *Lab Chip*, 11 (2011) 700-707.

[38] JE Hall. Guyton and hall textbook of medical physiology, twelfth ed. Saunders Elsevier, 2011.

[39] A Monkawa, T Ikoma, S Yunoki, K Ohta, and J Tanaka. Collagen coating on hydroxyapatite surfaces modified with organosilane by chemical vapor deposition method. *J Nanosci Nanotechnol*, 7 (2007) 833-838.

[40] RC Hooper, KA Hernandez, T Boyko, A Harper, J Joyce, AR Golas, and JA Spector. Fabrication and in vivo microanastomosis of vascularized tissue-engineered constructs. *Tissue Eng Part A*, 20 (2014) 2711-2719.

[41] N Lang, MJ Pereira, Y Lee, I Friehs, NV Vasilyev, EN Feins, K Ablasser, ED O'Cearbhaill, et al. A blood-resistant surgical glue for minimally invasive repair of vessels and heart defects. *Sci Transl Med*, 6 (2014) 218ra216.

[42] AN Makanya and V Djonov. Parabronchial angioarchitecture in developing and adult chickens. *J Appl Physiol (1985)*, 106 (2009) 1959-1969.